

## MIT Open Access Articles

*Interfacial viscoelasticity, yielding and creep  
ringing of globular protein–surfactant mixtures*

The MIT Faculty has made this article openly available. **Please share**  
how this access benefits you. Your story matters.

**Citation:** Jaishankar, Aditya, Vivek Sharma, and Gareth H. McKinley. Interfacial Viscoelasticity, Yielding and Creep Ringing of Globular Protein–surfactant Mixtures. *Soft Matter* 7(17): 7623. 2011.

**As Published:** <http://dx.doi.org/10.1039/c1sm05399j>

**Publisher:** Royal Society of Chemistry, The

**Persistent URL:** <http://hdl.handle.net/1721.1/79125>

**Version:** Author's final manuscript: final author's manuscript post peer review, without publisher's formatting or copy editing

**Terms of use:** Creative Commons Attribution-Noncommercial-Share Alike 3.0



# Interfacial viscoelasticity, yielding and creep ringing of globular protein-surfactant mixtures

Aditya Jaishankar, Vivek Sharma, and Gareth H. McKinley\*

Received Xth XXXXXXXXXXXX 20XX, Accepted Xth XXXXXXXXXXXX 20XX

First published on the web Xth XXXXXXXXXXXX 200X

DOI: 10.1039/b000000x

Protein-surfactant mixtures arise in many industrial and biological systems, and indeed, blood itself is a mixture of serum albumins along with various other surface-active components. Bovine serum albumin (BSA) solutions, and globular proteins in general, exhibit an apparent yield stress in bulk rheological measurements at surprisingly low concentrations. By contrasting interfacial rheological measurements with corresponding interface-free data obtained using a microfluidic rheometer, we show that the apparent yield stress exhibited by these solutions arises from the presence of a viscoelastic layer formed due to the adsorption of protein molecules at the air-water interface. The coupling between instrument inertia and surface elasticity in a controlled stress device also results in a distinctive damped oscillatory strain response during creep experiments known as “creep ringing”. We show that this response can be exploited to extract the interfacial storage and loss moduli of the protein interface. The interfacial creep response at small strains can be described by a simple second order system, such as the linear Jeffreys model, however the interfacial response rapidly becomes nonlinear beyond strains of order 1%. We use the two complementary techniques of interfacial rheometry and microfluidic rheometry to examine the systematic changes in the surface and bulk material functions for mixtures of a common non-ionic surfactant, Polysorbate 80, and BSA. It is observed that the nonlinear viscoelastic properties of the interface are significantly suppressed by the presence of even a relatively small amount of surfactant ( $c_{\text{surf}} > 10^{-3}$  wt.%). Preferential interfacial adsorption of the mobile surfactant at these surfactant concentrations results in complete elimination of the bulk apparent yield stress exhibited by the surfactant-free BSA solutions.

## 1 Introduction

Surface-active materials like proteins, low molecular weight surfactants and polymeric surfactants adsorb to fluid interfaces, effectively reducing the interfacial tension, and endowing the interface with additional independent material properties such as surface elasticity and viscosity<sup>1,2</sup>. The dynamic interfacial properties of these adsorbed interfacial layers are important for a number of technological applications including foam and emulsion formation and stabilization in food processing<sup>3,4</sup>, cosmetics and pharmaceutical industry<sup>4,5</sup>. The interfacial viscoelasticity also plays an important role in spray coating, Langmuir-Blodgett deposition, liquid-liquid deposition, two phase flows and mass transfer<sup>1,2</sup>. Multicomponent mixtures of proteins and surfactants are used in many of these applications, and are also commonly found in many biological systems<sup>6–8</sup> including blood: a mixture of serum albumins along with various other surface-active components<sup>6,8</sup>. The addition of surfactants to protein solutions can substantially modify the physiochemical properties of the resulting interface<sup>2,6,9–11</sup>. For example, the interfacial shear viscos-

ity (which characterizes resistance to changes in shape at constant area on a two-dimensional interface), is affected by the structure, composition and conformation of the interfacial components of these mixed systems<sup>3,6,9,10,12</sup>. In this study, we focus on the interfacial and bulk rheology of a protein-surfactant mixture, using solutions of a model globular protein, Bovine Serum Albumin (BSA), mixed with a non-ionic surfactant polysorbate 80 (or Tween 80<sup>TM</sup>). We specifically choose Bovine serum albumin (BSA) for our study because its physical properties and diverse biological functions are similar to Human serum albumin (HSA)<sup>13,14</sup>.

When the rheological properties of globular protein solutions such as BSA are tested in a torsional rheometer, they exhibit yield-like behaviour at surprisingly low concentrations (0.03%–10%)<sup>15–20</sup>, and show pronounced shear thinning at low shear rates. This has been attributed in past studies<sup>15–17</sup> to the presence of long ranging colloidal forces that are stronger than electrostatic interactions, and which lead to an ordered bulk colloidal structure formation. In a recent paper<sup>20</sup>, we demonstrated that this apparent bulk yield stress and the associated shear thinning rheological response in fact arises from the presence of a viscoelastic layer formed due to protein adsorption at the air-water interface. We used the recently-developed interfacial double wall ring (DWR)<sup>21</sup> fix-

Hatsopoulos Microfluids Laboratory, Department of Mechanical Engineering, Massachusetts Institute of Technology, Cambridge, MA 02139 USA. E-mail: [gareth@mit.edu](mailto:gareth@mit.edu)

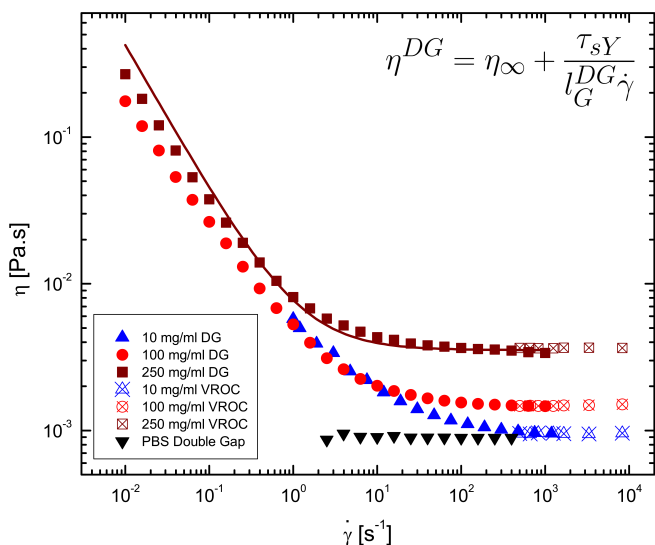


**Fig. 1** Comparison of steady shear viscosity of different concentrations of BSA solutions in the double gap Couette geometry (filled symbols) and interface-free microfluidic rheometer (crossed symbols). The solid line shows the prediction of the simple two parameter model for the 250 mg/ml sample with a purely viscous sub-phase ( $\eta_{\infty} = 3.53 \times 10^{-3}$  Pa s) and a purely plastic interface ( $\tau_{sY} = 2.5 \times 10^{-4}$  Pa m).

ture mounted on a stress-controlled rheometer to carry out a series of interfacial rheological measurements in steady and oscillatory shear. We augmented these measurements with bulk and interface-free microfluidic rheometry data to highlight the strong influence that the interfacial layer has on bulk rheology. A detailed description of the instruments and setup is provided in the methods section. As an example, the shear-rate-dependent steady shear viscosity  $\eta^{DG}(\dot{\gamma})$  for different concentrations of BSA measured in a double gap Couette geometry on a torsional rheometer (filled symbols) and in an interface-free microfluidic capillary viscometer device  $\eta_{\infty}(c)$  (crossed symbols) is shown in Figure 1, adapted from Sharma et al.<sup>20</sup>. The total torque measured by the rheometer is the sum of a sub-phase contribution and an interfacial contribution. A simple additive model (shown by the solid line) captures the rate-dependence of the measured bulk viscosity closely. This model treats the adsorbed protein layer as a pure elasto-plastic material that undergoes yielding beyond a critical strain, and for the range of BSA concentrations studied, the interfacial contribution to the stress is dominated by the interfacial yield stress  $\tau_y$  of the viscoelastic layer (which is measured independently using the DWR). The measured bulk viscosity  $\eta(\dot{\gamma})$  can then be written as the sum of the rate-independent Newtonian viscosity of the globular protein solution  $\eta_{\infty}(c)$  and the con-

tribution from the interface as:

$$\eta^{DG}(\dot{\gamma}) = \eta_{\infty}(c) + \frac{\tau_{sY}}{l_G^{DG} \dot{\gamma}} \quad (1)$$

Where  $l_G^{DG}$  is the geometry-dependent length scale of the double gap geometry. For a more detailed derivation and a more extensive background, the interested reader is referred to this work<sup>20</sup>.

Every surface-active material that forms a viscoelastic film at the liquid-air interface can lead to a measurable apparent yielding behavior, as long as the interfacial yield stress (the second term in Equation (1)) is significant. The presence of an apparent yield stress in the bulk rheological measurement is also reported for solutions of ovalbumin<sup>22</sup>, saliva<sup>23</sup>, monoclonal antibodies<sup>24</sup> and acacia gum<sup>25</sup>. In practice, the interfacial contribution from surface-active components in multi-component fluids can be suppressed by the addition of a low molecular-weight mobile surfactant, which competes with the protein for adsorption onto the interface<sup>2,11,26–30</sup>. The irreversibility of the adsorption, the presence of heterogeneous domains, significant interfacial phase separation at the interface and the sensitivity of the structure of the interfacial layer to the adsorption history make accurate measurements a challenging task<sup>3,4,31</sup>. Given these challenges, a simple experimental protocol that provides a check for the presence of surface viscoelasticity and an estimate of its magnitude in protein-surfactant mixtures will be of broad utility.

In this study, we examine the bulk and interfacial rheological response of protein-surfactant mixtures, specifically to evaluate how the addition of a surfactant to a protein solution changes the dynamical properties of the interface. We first review the concept of creep ringing or “free-oscillations” in creep experiments under constant stress. We then show how this inertio-elastic effect impacts interfacial creep measurements performed with the DWR interfacial fixture, and how it can be exploited to make quick and accurate measurements of viscoelastic moduli for Bovine Serum Albumin (BSA) solutions. We compare these measurements with interfacial small amplitude oscillatory strain experiments (SAOS) and then study the effect of adding a non-ionic surfactant (polysorbate 80) to the BSA solutions using the creep-ringing technique.

## 2 Experimental

### 2.1 Materials

Bovine Serum Albumin, extracted by agarose gel electrophoresis, was obtained from Sigma-Aldrich Corp, St. Louis, MO USA, in the form of a lyophilized powder. 0.01 M Phosphate Buffered Saline (PBS) Solution (NaCl-0.138 M;

KCl-0.0027 M; pH 7.4, at 25°C.), was prepared by dissolving dry PBS powder obtained from Sigma-Aldrich Corp. A weighed quantity of BSA was dissolved in the PBS and the solution was brought up to the required volume in a volumetric flask to finally obtain solutions with a BSA concentration of 50 mg/ml. BSA was weighed in an Excellence XS64 Analytical Balance (Mettler-Toledo AG, Greifensee, Switzerland) with a resolution of 0.1 mg. Mixtures were always prepared in batches of 100 ml, so that the amount of BSA to be weighed was large and the error was reduced (50 mg/ml x 100 ml = 5 g ± 0.1 mg). In this manner, the uncertainty in weight was only 0.002%. The prepared solutions were stored under refrigeration at 4°C and were allowed to warm up to room temperature before being used for experiments. All BSA solutions used in this study had a concentration of 50 mg/ml unless otherwise specified, which is the same as the concentration of Human Serum Albumin in human blood<sup>14</sup>.

The surfactant used in this study was polysorbate 80 (Tween 80™, P1754, Sigma-Aldrich Corp.). To prepare the protein-surfactant mixtures, a known amount of polysorbate 80 was weighed and dissolved in PBS. This was then dissolved into a weighed amount of BSA solution to achieve the required concentration. To increase accuracy, solutions with  $c_{\text{surf}} \leq 10^{-3}$  wt.% were prepared by successive dilution. We chose a non-ionic surfactant because additional complications can arise due to complex formation between BSA and ionic surfactant molecules. If there is a favorable interaction between the protein and the surfactant, the protein can adopt a very different conformational state as compared to the native protein<sup>2,6,32</sup>.

## 2.2 Methods

Bulk and interfacial steady shear and oscillatory measurements were performed using a stress-controlled torsional rheometer (TA Instruments AR-G2). Bulk measurements were performed using a double gap (DG) Couette fixture, while interfacial experiments were performed using the double wall ring (DWR) geometry, described in detail by Vandebriel et al.<sup>21</sup>. The DWR is an annular ring with a diamond cross-section made of a platinum-iridium alloy that sits at the air-liquid or liquid-liquid interface and undergoes in-plane torsional displacements.

When performing interfacial rheology measurements, it is important to understand the relative contributions of the sub-phase and interfacial flows to the total resistive torque measured by the rheometer. The selective sensitivity of a specific test geometry to interfacial effects, in comparison to the induced sub-phase flow is described by the Boussinesq Number  $Bo_s$  which is defined as<sup>1</sup>,

$$Bo_s = \frac{\text{Surface Drag}}{\text{sub-phase Drag}} = \frac{(\eta_s V / L_s) P_s}{(\eta V / L_B) A_B} = \frac{\eta_s}{\eta L_s} \quad (2)$$

where  $\eta_s$  is the interfacial viscosity,  $V$  is a characteristic velocity, and  $L_s$  and  $L_B$  are characteristic length scales over which the interfacial and bulk flows decay respectively,  $P_s$  is the perimeter of contact between the geometry and the fluid interface, and  $A_B$  is the area of contact between the geometry and the underlying fluid sub-phase. The length scale  $L_s$  is thus critical in determining the sensitivity of a specific test fixture to interfacial effects, and to ensure  $Bo_s \gg 1$  for a wide range of fluids, we require small values for  $L_s$ . The DWR geometry minimizes the length scale  $L_s$  by maximizing the wetted perimeter for a given contact area. For example, for the specific DWR fixture used in the present study, we calculate  $L_s^{\text{DWR}} = 0.7$  mm. By contrast, for a 40 mm diameter 2° cone,  $L_s^{\text{CP}} = 10$  mm and for the double gap Couette used in this study,  $L_s^{\text{DG}} = 59.5$  mm. This makes the DWR especially suited for interfacial rheology compared to other regular geometries like the cone-and-plate or the double gap Couette geometry.

To correct for any torque contributions arising from the induced sub-phase flow, we corrected all of our measurements for non-linearity using the MATLAB script described by Vandebriel et al.<sup>21</sup> (kindly provided by Jan Vermant, K.U. Leuven, Belgium), and confirmed that this correction did not make any appreciable difference to the measured data for the range of interfacial properties that characterize the BSA solutions studied here. (see Figure SI.8 of the supplementary information<sup>20</sup> and the discussion therein.) While nearly no sub-phase corrections are required for the data measured using the DWR geometry, in other instruments used for making interfacial measurements with lower characteristic values of the Boussinesq numbers, the sub-phase contributions to the torque must be carefully accounted for (see, for example, the papers by Mannheimer and Schechter<sup>33</sup> and Oh and Slattery<sup>34</sup>). Several studies<sup>3,4,31,35</sup> have noted the long time scales required for adsorbed interfacial layers to reach equilibrium, with Wierenga et al.<sup>35</sup> waiting for as long as 24 hours. This effect is even more pronounced in surfactant-protein mixtures<sup>31,36</sup>. Based on preliminary time sweep experiments and a consideration of evaporation times, all steady state experiments were performed with a waiting time of around 3 hours. The transient evolution of the surface properties is also discussed briefly in the results section.

Complementary bulk rheological measurements were carried out using a double gap circular Couette (DG) geometry (rotor inner radius = 20.38 mm, rotor outer radius = 21.96 mm, rotor height = 59.5 mm, cup inner radius = 20 mm) attached to the controlled-stress rheometer. To examine the role played by the interface and the effect of added surfactant in bulk rheological measurements, experiments were also performed using an interface-free microfluidic capillary rheometer, (mVROC Viscometer-Rheometer-on-a-chip, manufactured by Rheosense Inc., San Ramon, CA). Specifically, in the present study the Type A05 chipset was used, which con-

sists of a rectangular cross-section channel (width  $w = 3.02$  mm; depth  $d = 50 \mu\text{m}$ ) fabricated from Pyrex, mounted on a gold-coated silicon base containing three flush mounted pressure sensors<sup>37</sup>. The nominal wall shear rate is given by  $\dot{\gamma}_w = 6Q/wd^2$  where  $Q$  is the volume flow rate through the channel. The pressure drop  $\Delta P$  along the channel is related to the wall shear stress  $\tau_w$  by the force balance  $wd\Delta P = 2\tau_w(w+d)l$ , where  $l$  is the length of the channel. The viscosity is then calculated in the usual manner and is given by  $\eta = \tau_w/\dot{\gamma}_w$ . The maximum attainable pressure  $P_{\text{max}}$  measurable in the mVROC type A05 chip is  $P_{\text{max}} = 14$  kPa. The minimum sensitivity of this sensor is 1% full scale, and hence  $P_{\text{min}} = 140$  Pa. In calculating  $\dot{\gamma}_w$ , a parabolic fully-developed profile is assumed within the channel. This is true for a Newtonian fluid, but the velocity profile deviates from parabolic if the fluid used is non-Newtonian. In such a case, the Weissenberg-Rabinowitsch-Mooney (WRM) equation can be used to calculate the true shear rate from the nominal shear rate  $\dot{\gamma}_w$  defined above<sup>37</sup>. We recalculated our data using the WRM equation and the results changed by less than 1%, signifying that the behavior of the BSA-surfactant mixtures in the channel is indeed Newtonian.

### 2.3 Creep Ringing in Bulk Rheology

Inertial effects are almost always unavoidable in controlled-stress rheometry, especially in step-stress and impulse-response experiments<sup>38</sup>. The angular acceleration of the fixture is retarded by the moment of inertia  $I$  (units:  $\text{kg m}^2$ ) of the spindle of the torsional rheometer, and the attached geometry. The coupling between this moment of inertia and the fluid viscoelasticity is seen in the general equation of motion of the fluid in step-stress experiments<sup>39</sup>

$$\frac{I}{b}\ddot{\gamma} = H(t)\tau_0 - \tau(t) \quad (3)$$

Where  $\gamma(t)$  is the strain in the sample,  $H(t)$  is the Heaviside step function,  $\tau_0$  is the magnitude of the step in the applied stress and  $\tau(t)$  is the retarding stress exerted by the sample on the fixture. The double over-dot indicates the second derivative with respect to time. The parameter  $b = F_\gamma/F_\tau$  is a combination of geometric factors (units:  $\text{m}^3$ ) and is determined by the specific instrument and geometry used. The factors  $F_\gamma = \dot{\gamma}/\Omega$  (dimensionless) and  $F_\tau = \tau/T$  (units:  $\text{m}^{-3}$ ) are geometric parameters that convert the measured variables of angular velocity  $\Omega$  and torque  $T$  to shear rate  $\dot{\gamma}$  and shear stress  $\tau$  respectively. It can instantly be seen from Equation (3) that due to the non-zero inertia of the system,  $\tau(t) \neq H(t)\tau_0$ .

For a Newtonian fluid with viscosity  $\eta$ ,  $\tau(t) = \eta\dot{\gamma}(t)$ , and in the absence of inertia, the solution to Equation 3 gives the expected linear response  $\gamma(t) = (\tau_0/\eta)t$ . However, for non-

zero inertia, the strain  $\gamma(t)$  is given by

$$\gamma(t) = \frac{\tau_0}{\eta} \left[ t - \frac{I}{b\eta} \left( 1 - \exp\left(-\frac{b\eta}{I}t\right) \right) \right] \quad (4)$$

The characteristic time constant for this exponential response is  $t_c = I/b\eta$ . At long times  $t > 3I/b\eta$  the expected linear system response is recovered but the strain is retarded by a factor  $I/b\eta$  and  $\gamma(t) = (\tau_0/\eta)(t - t_c)$ . For  $t \ll I/b\eta$ , the exponential term in Equation 4 can be expanded to obtain  $\gamma(t) = (\tau_0 b/2I)t^2 + O(t^3)$  and hence the short time response is quadratic as expected from Newton's second law. It should be noted that this short-time creep response is independent of the fluid rheology and is valid for all test fluids at sufficiently early times.

When the equation of motion (Equation 3) is coupled with a viscoelastic constitutive model, the presence of the inertial term leads to a damped oscillatory response during creep experiments. (See references<sup>39,40</sup> and the Results section of this paper for the exact form of this strain response). These oscillatory dynamics often cloud the short time creep response and are generally considered undesirable. However, Struik and others have described procedures from which one can extract bulk viscoelastic storage and loss moduli using this 'creep-ringing' or free oscillation<sup>40,41</sup>. In the present study, we show how this bulk analysis can also be adapted in order to use creep ringing measurements with the DWR fixture to extract the interfacial viscoelastic properties of an adsorbed protein film. Larsen et al. have observed creep ringing while studying the interfacial properties of a metal oxide film<sup>42</sup>. However, their analysis does not include the coupling of the inertia equation (3) with a viscoelastic model. In this paper, we adapt the bulk creep ringing formulation outlined above to the extraction of interfacial moduli using a three-parameter linear viscoelastic Jeffreys model.

## 3 Results and Discussion

### 3.1 Interfacial Creep Ringing Theory

We begin with the equation of motion for the DWR fixture and associated spindle, and derive the interfacial counterpart of Equation 3 to be<sup>43</sup>:

$$\frac{I}{b_s}\ddot{\gamma} = H(t)\tau_0^s - \tau_s \quad (5)$$

The subscript  $s$  denotes a surface or interfacial quantity. For a step-stress or creep experiment, the applied interfacial stress is  $H(t)\tau_0^s$ , where  $\tau_0^s$  is the magnitude of the step in the interfacial stress. We note that the interfacial measurement system factor  $b_s = F_\gamma/F_\tau$  now has units of  $\text{m}^2$ , since the interfacial stress  $\tau_s$  is a force per unit length and has units of  $\text{N m}^{-1}$  or  $\text{Pa m}$ .

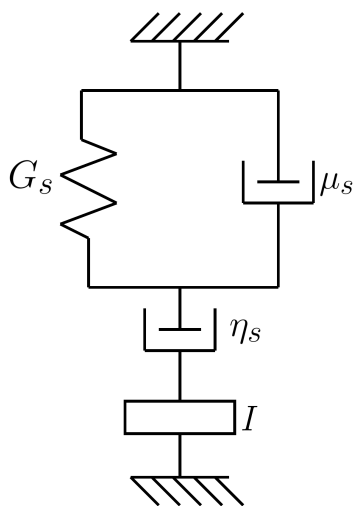


**Fig. 2** A schematic diagram of the linear viscoelastic Jeffreys model, which consists of a spring and a dashpot in parallel (Kelvin-Voigt element) in series with a dashpot. Note the addition of the fourth element  $I$  which represents the instrument inertia and is the source for creep ringing.

To solve this equation of motion for the DWR fixture (Equation 5), an appropriate rheological constitutive equation for the interface must be selected. Following the corresponding bulk formulations of Baravian and Quemada<sup>40</sup> and Ewoldt et al.<sup>39</sup>, we model the interfacial layer of globular protein using a three-parameter linear viscoelastic Jeffreys model, shown in Figure 2. The model consists of a Voigt element (a spring and dashpot in parallel) in series with a dashpot;  $G_s$  (units: Pa m),  $\mu_s$  and  $\eta_s$  (units: Pa s m) are the three parameters in the model. At long times, the Voigt element attains a steady deformation when loaded under controlled stress conditions and hence the remaining dashpot ( $\eta_s$ ) leads to a fluid-like response of the adsorbed protein interface ( $\gamma(t) = (\tau_0^s/\eta_s)t$ ). Conversely, taking the Kelvin-Voigt model alone, for example, would give a constant strain at long times and hence a solid-like interfacial response. Since we observe a steady-state flow at long times during our interfacial creep experiments (see the next subsection), we use the Jeffreys model to fit our data. Tschoegl<sup>44</sup> provides a detailed discussion on these simple two- and three-parameter models as well as more complex multiparameter models, and the reader is referred there for more information.

For the Jeffreys model, the constitutive equation is,

$$\left(1 + \frac{\mu_s}{\eta_s}\right) \dot{\tau}_s + \frac{G_s}{\eta_s} \tau_s = G_s \dot{\gamma} + \mu_s \ddot{\gamma} \quad (6)$$

Equation 6 is then coupled with Equation 5 to obtain the full

equation of motion for the DWR fixture

$$\left(1 + \frac{\mu_s}{\eta_s}\right) \dot{\gamma} + \left[\frac{G_s}{\eta_s} + \frac{\mu_s}{I/b_s}\right] \dot{\gamma} + \frac{G_s}{I/b_s} \gamma = \frac{G_s}{\eta_s(I/b_s)} \tau_0^s t + \frac{1 + \mu_s/\eta_s}{I/b_s} \tau_0^s H(t) \quad (7)$$

This second order differential equation can be solved explicitly to find the strain as a function of time<sup>39</sup>:

$$\gamma(t) = \frac{\tau_0^s}{\eta_s} t - B + e^{-At} \left[ B \cos(\omega t) + \frac{A}{\omega} \left( B - \frac{\tau_0^s}{\eta_s A} \right) \sin(\omega t) \right] \quad (8)$$

where

$$\omega = \sqrt{\frac{G_s}{\alpha_s} \frac{\eta_s}{\mu_s + \eta_s} - A^2} \quad (9)$$

$$A = \frac{G_s/\eta_s + \mu_s/\alpha_s}{2(1 + \mu_s/\eta_s)} \quad (10)$$

$$B = \frac{\tau_0^s}{G_s} \frac{\eta_s + \mu_s}{\eta_s} \left( \frac{2A\alpha_s}{\eta_s} - 1 \right) \quad (11)$$

Here, we introduce the factor  $\alpha_s = I/b_s$  (units: kg m<sup>2</sup>/m<sup>2</sup>=kg) for compactness. The viscoelastic storage modulus  $G'_s$  and loss modulus  $G''_s$  for the Jeffreys model are given respectively by the following expressions<sup>39</sup>

$$G'_s = G_s \frac{(\lambda_2 \omega)^2}{1 + (\lambda_1 \omega)^2} \quad (12)$$

$$G''_s = G_s \frac{(\lambda_2 \omega) [1 + (\lambda_1^2 - \lambda_1 \lambda_2) \omega^2]}{1 + (\lambda_1 \omega)^2} \quad (13)$$

where  $\lambda_1 = (\mu_s + \eta_s)/G_s$  and  $\lambda_2 = \eta_s/G_s$  are the relaxation time and retardation time respectively. For creep ringing to be observed, the system response to Equation 7 needs to be under-damped, and hence we require  $G_s > G_{\text{critical}} = A^2 \alpha_s (1 + \mu_s/\eta_s)$ . Under these conditions, data from creep experiments can then be fitted with Equation 8 and the interfacial storage and loss modulus of the interface can be calculated using Equations 12 and 13 after a least square fit over  $G_s$ ,  $\mu_s$  and  $\eta_s$  is carried out. Alternatively, Struik has demonstrated that, under certain conditions (given below), the linear moduli can be approximated directly by using the logarithmic decrement and the frequency of the creep ringing<sup>41</sup>. Because Equation 5 is identical to the equation of motion for free oscillations of a standard torsional device, we can readily adapt Struik's formulae to obtain the following expressions for the interfacial viscoelastic moduli:

$$G'_s \approx \alpha_s \omega_*^2 \left[ 1 + \left( \frac{\Delta}{2\pi} \right)^2 \right] \quad (14)$$

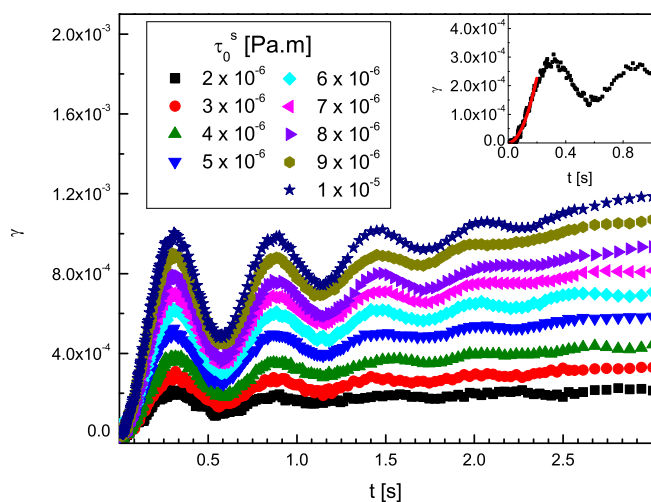


**Fig. 3** Interfacial creep ringing experiments performed on 50 mg/ml BSA using the DWR (double wall ring) geometry attached to a stress controlled rheometer (AR-G2) for different values of applied interfacial stress  $\tau_0^s$ . While the amplitude of creep ringing increases with increasing stress, the ringing frequency remains the same. The inset shows the short time response for  $\tau_0^s = 3 \times 10^{-6}$  Pa m. The red line is a quadratic fit to the short time response. The measured value of  $\alpha_s^{(m)} = 1.85 \times 10^{-4}$  kg extracted from the fit is in close agreement with the calculated value of  $\alpha_s^{(c)} = 1.72 \times 10^{-4}$  kg.

$$G_s'' \approx \alpha_s \omega_*^2 \left( \frac{\Delta}{\pi} \right) \quad (15)$$

$$\tan \delta \approx \frac{\Delta/\pi}{1 + \left( \frac{\Delta}{2\pi} \right)^2} \quad (16)$$

where  $\delta$  is the phase angle,  $\omega_*$  is the ringing frequency (units:  $\text{rad s}^{-1}$ ) and  $\Delta = \ln(A_{n+1}/A_n)$  is the logarithmic decrement, (with  $A_n$  being the amplitude of the  $n^{\text{th}}$  peak or trough). These expressions provide estimates for the linear viscoelastic moduli without the assumption of an underlying model provided the logarithmic decrement  $\Delta$  is small, and the instrument compliance and fluid inertia are negligible.

### 3.2 Interfacial Creep Ringing of BSA Solutions

To extract the viscoelastic storage and loss moduli for the BSA solutions, we used the interfacial creep ringing procedure outlined above. Using the Double Wall Ring (DWR) fixture, we measured the strain response as a function of time for different values of interfacial stress  $\tau_0$  in creep experiments as shown in Figure 3. The coupling between surface elasticity and instrument inertia leads to the periodic and exponentially decaying oscillations seen for  $t \leq 2$  s, expected from Equation 8. Although the amplitude of the oscillations increases with the magnitude of the imposed stress  $\tau_0^s$ , the frequency of

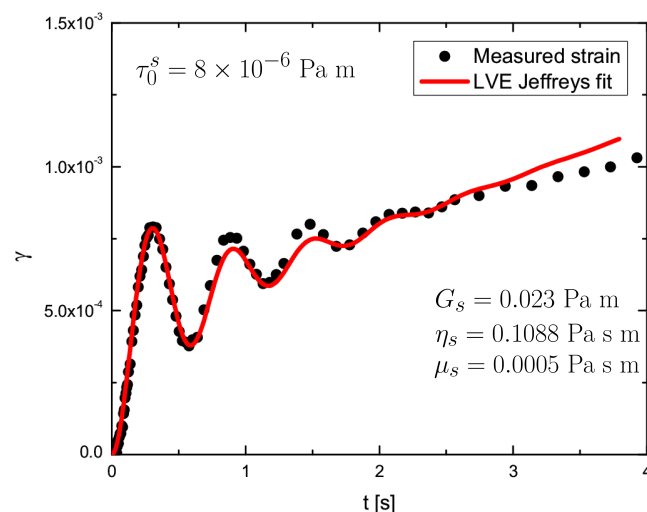


**Fig. 4** Fit of a linear viscoelastic Jeffreys model to the short time response of an interfacial creep experiment. While the short time ringing response is fit well by this model, the beginning of deviations from linearity can be seen for  $t > 3$  s.

ringing is determined only by the surface viscoelasticity and the geometry of the DWR (see Equations 14 and 15). The inset to Figure 3 shows the short time response for a creep experiment performed at  $\tau_0^s = 3 \times 10^{-6}$  Pa m. Using a Taylor series expansion of Equation 8, and neglecting cubic and higher order terms, it can be shown that for short times that  $\gamma(t) \approx (\tau_0^s/2\alpha_s)t^2$  and the short-time response is quadratic in time, as anticipated in Equation 4. Fitting a pure quadratic polynomial to the measured short time creep response (red line in the inset of Figure 3), we find  $\alpha_s^{(m)} = 1.85 \times 10^{-4}$  kg (the superscript  $m$  signifies that this is a measured quantity). The parameter  $\alpha_s = I/b_s$  is a characteristic parameter of the instrumentation, since the total moment of inertia of the system  $I$  can be calibrated independently, and the factor  $b_s = F_\gamma/F_\tau$  is determined by the geometry being used (for the DWR used in this study,  $F_\gamma = 9.393$  and  $F_\tau = 64.94 \text{ m}^{-2}$  giving  $b_s = 0.144 \text{ m}^2$ ). For the experimental configuration used here,  $\alpha_s^{(c)}$  was calculated to be  $\alpha_s^{(c)} = 1.72 \times 10^{-4}$  kg (the superscript  $c$  signifies this is a calculated quantity). Using this value of  $\alpha_s$ , Equations 14 and 15 were used to estimate the interfacial viscoelastic moduli from the logarithmic decrement method and we have  $G_s' \approx 0.021 \text{ Pa m}$  and  $G_s'' \approx 3.8 \times 10^{-3} \text{ Pa m}$  respectively. Hence, from a single creep experiment, both the inertia of the measurement system as well as the viscoelasticity of the adsorbed interfacial protein layer can be determined.

A fit of the linear viscoelastic Jeffreys model (Equation 8) to the interfacial creep ringing experiment with  $\tau_0^s = 8 \times 10^{-6}$  Pa m was carried out with MATLAB and is shown in Figure 4. From the fit parameters, the interfacial storage and loss

moduli can be calculated using Equations 12 and 13 to give  $G'_s \approx 0.022 \text{ Pa m}$  and  $G''_s \approx 4.4 \times 10^{-3} \text{ Pa m}$  respectively. We see that the fit to the Jeffreys model is good at short times, but progressive deviations from linearity are seen for  $t > 3 \text{ s}$  as the total strain accumulated by the interface increases.

To investigate the onset of nonlinearity, small amplitude oscillatory strain sweeps and frequency sweeps with the DWR fixture were also performed and are presented in Figures 5a and 5b. In Figure 5a, the onset of nonlinear response in the viscoelastic interfacial layer can be seen to occur at a strain amplitude of  $\gamma_0 \approx 2\%$ . For  $\gamma_0 \leq 2\%$ , the interfacial elastic modulus  $G'_s$  is larger than the interfacial loss modulus  $G''_s$ , indicating that the interfacial layer exhibits viscoelastic solid-like properties at small/moderate strains. The rapid collapse in the magnitude of  $G'_s$  and the dominance of the viscous response  $G''_s$  for strains beyond  $\gamma_0 \sim 5\%$  is indicative of a yielding process in the interfacial film. We note that the values of  $G'_s$  and  $G''_s$  obtained from the damped free-oscillation measurements during creep ringing and the value extracted from the fit to the Jeffreys model (Equation 8) agree well with the corresponding SAOS measurements at the appropriate frequency  $\omega_*$ . These values are summarized in Table 1. From the crossover fre-

**Table 1** Values of interfacial viscoelastic moduli for 50 mg/ml BSA solutions obtained by the three independent methods described in the text; namely a fit to the linear Jeffreys model (Equations 12 and 13), evaluation of the logarithmic decrement (Equations 14 and 15), and small amplitude oscillatory interfacial shear flow (SAOS, Figure 5)

Quantity [Pa m]	Log Decrement	Jeffreys fit	SAOS
$G'_s$	0.021	0.022	0.022
$G''_s$	$3.8 \times 10^{-3}$	$4.4 \times 10^{-3}$	$4.6 \times 10^{-3}$

quency in Figure 5b, the relaxation time of the viscoelastic BSA interface was estimated to be  $\lambda = 6.5 \text{ s}$ .

A strong case for using creep ringing observations to estimate the viscoelastic properties of the interfacial film is made from the inertial effects seen for  $\gamma_0 > 20\%$  in Figure 5a and for  $\omega > 20 \text{ rad s}^{-1}$  in Figure 5b. The raw phase angle exceeds  $170^\circ$  for these values of strain and frequency (filled blue triangles), indicating the onset of inertial effects. These can corrupt the experimental data and limit the range of measurable frequencies or strains in a small amplitude oscillatory measurement. Baravian and Quemada<sup>40</sup> have pointed out that creep ringing extends the range of measurable frequencies in a frequency sweep test. Because interfacial creep ringing accounts for, and in fact exploits, the finite moment of inertia of the measurement system, the range of measurable frequencies is extended beyond what is possible in a standard frequency sweep. From Equation 8, we see that  $\omega_*$  varies inversely with  $\alpha_s$ , which in turn depends on the geometric factor  $b_s$  and hence designing appropriate interfacial geometries with smaller val-

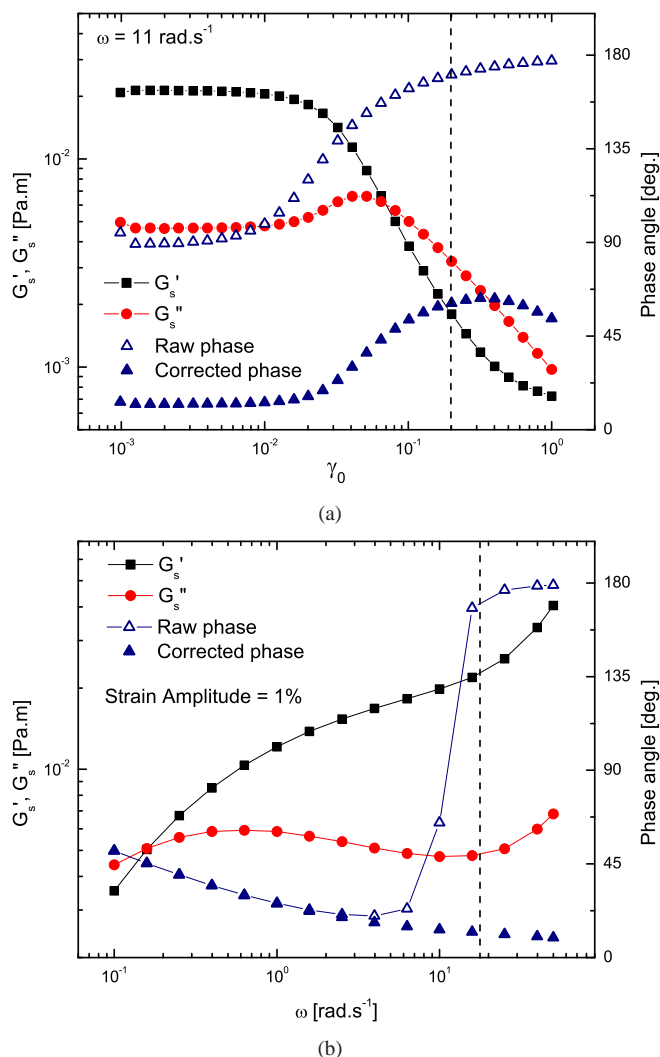


**Fig. 5** (a) Interfacial small amplitude oscillatory strain sweep for 50 mg/ml BSA performed at angular frequency  $\omega = 11 \text{ rad s}^{-1}$ . Beyond a strain amplitude of  $\gamma_0 = 2 \times 10^{-2}$  (2%), the interfacial film yields plastically. In the linear viscoelastic region,  $G'_s = 0.022 \text{ Pa m}$ . Inertial effects, which are detrimental in an SAOS experiment and corrupt the measurement, can be seen for  $\gamma_0 > 20\%$  (region to the right of the dashed line). (b) Interfacial small amplitude oscillatory frequency sweep for 50 mg/ml BSA solution with  $\gamma_0 = 1\%$ . At  $\omega = 10 \text{ rad s}^{-1}$ ,  $G'_s = 0.021 \text{ Pa m}$ . Again, inertial effects become dominant in the region to the right of the dashed line ( $\omega > 20 \text{ rad s}^{-1}$ ). From the crossover frequency, the relaxation time  $\lambda$  is estimated to be  $\lambda \approx 6.5 \text{ s}$ .



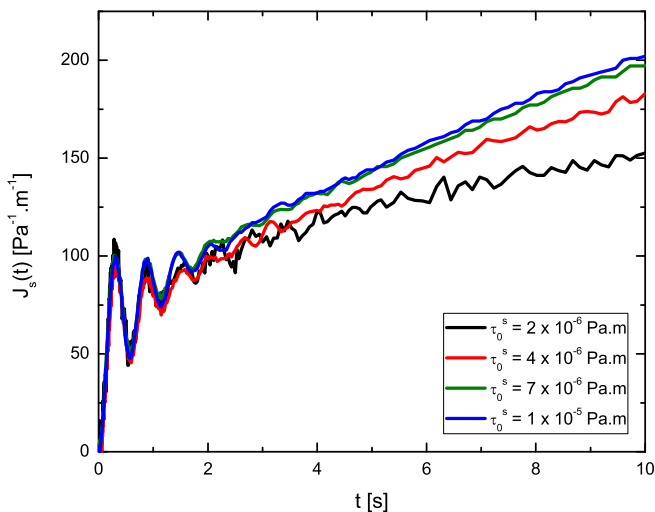


**Fig. 6** Comparison of interfacial creep compliance  $J_s(t) = \gamma(t)/\tau_0^s$  for different values of interfacial stress  $\tau_0^s$  performed on 50 mg/ml BSA solutions. For an ideal linear material, all curves collapse onto each other. Although the short time creep compliances collapse, deviations can be seen at long times, indicating onset of non-linear behavior.

ues of  $\alpha_s$  enables one to probe progressively higher frequencies without inertial distortions like those seen in Figure 5. We note that the local peak in  $G_s''$  seen in Figure 5a around  $\gamma_0 \approx 2\%$  is unrelated to the onset of inertia.

The interfacial creep compliance  $J_s(t) = \gamma(t)/\tau_0^s$  for different values of interfacial stress  $\tau_0^s$  is shown in Figure 6. For an ideal linear viscoelastic material, the compliance curves will all collapse onto each other. Moreover, for the linear Jeffreys model, the third term in Equation 8 is negligible at long times, and the strain will increase linearly with time. Inspection of Figure 6 shows that neither of these conditions is satisfied for the BSA interface at large strains. While the compliance curves all collapse at short times (in the region where creep ringing is present), they deviate progressively from each other for  $t \geq 5$  s. Figure 7 shows the strains measured during creep experiments performed at two different stress values on a log-log scale. At long times, the strain response of each curve deviates from linearity to different extents, with interfacial creep compliances given by  $J_s(t)|_{\tau_0^s=2 \times 10^{-6}} \sim t^{0.28}$  and  $J_s(t)|_{\tau_0^s=1 \times 10^{-5}} \sim t^{0.45}$  respectively. The inset to the figure shows the power-law indices obtained for creep experiments at different values of interfacial stress  $\tau_0^s$ . The indices approach a constant value of  $n = 0.45 \pm 0.04$  as  $\tau_0^s$  is increased. This power-law creep response in time cannot be described by any simple linear viscoelastic model. The Voigt element shown in Figure 2 approaches a steady deformation at long times, and hence the interfacial stress arises solely from the second dashpot (with viscosity  $\eta_s$ ) that is in series with the Voigt ele-

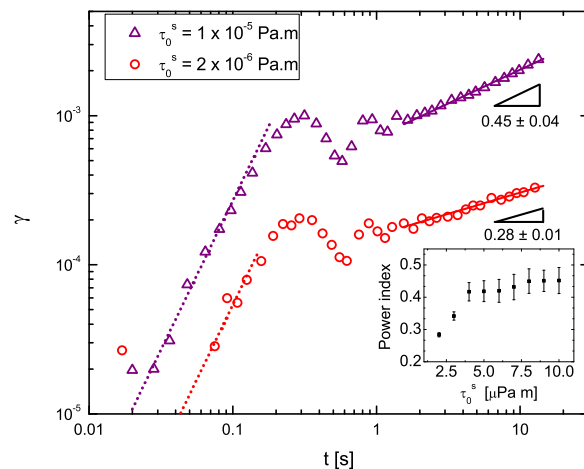


**Fig. 7** Strain  $\gamma(t)$  measured in an interfacial creep experiment on 50 mg/ml BSA solutions at different applied stresses  $\tau_0^s = 2 \times 10^{-6}$  Pa m and  $\tau_0^s = 1 \times 10^{-5}$  Pa m. The solid lines show a power law fit to the creep data for  $2 \text{ s} < t < 10 \text{ s}$  for experiments performed at two different stresses. The nonlinearity in the material response at large strains is clearly visible, with both slopes deviating from a slope of unity. The dotted lines show the quadratic response given by  $\gamma_0 = (\tau_0^s b_s / 2I) t^2$  for short times  $t < 0.1$  s. The inset plot shows the value of the power-law indices at different interfacial stress values  $\tau_0^s$ .

ment. A similar asymptotic response can be deduced for any other, more complex arrangement of linear springs and dashpots in parallel. To describe a power-law creep response, a more complex constitutive model containing 'springpot' mechanical elements and incorporating fractional derivatives is required<sup>44,45</sup>.

An examination of the parameter fits obtained from the measured creep response in Figures 4 shows that  $\mu_s \ll \eta_s$ . In this limit, the material description of the interface reduces to a linear Maxwell model ( $\mu_s \rightarrow 0$  in Figure 2 and Equations 6-13). This considerably simplifies the evaluation of the linear viscoelastic interfacial moduli and shows that for small strains at least, the interfacial protein layer is modeled well by the simplest linear viscoelastic model.

Interfacial creep experiments have been discussed in a number of studies in the past<sup>7,46-49</sup>. However, none of these studies reports the distinct periodic oscillations seen during creep ringing. As mentioned before, to observe creep ringing, we require  $G_s > G_{\text{critical}} = A^2 \alpha_s (1 + \mu_s / \eta_s)$ . From this expression, we see that a high interfacial elastic modulus, combined with a low instrument inertia increases the the possibility of visible creep ringing. The double wall ring used in this study has a lower moment of inertia compared to bulk geometries like a cone-and-plate. Also, the interfacial layer formed by BSA is stiff and elastic. These two factors in conjunction are responsible for the manifestation of the creep ringing response

described in the present study.

### 3.3 Protein-Surfactant Mixtures

The bulk shear viscosity of protein-surfactant (BSA-polysorbate 80) solutions measured using the microfluidic rheometer is shown in Figure 8a for 50 mg/ml BSA solutions with different concentrations of added surfactant. The behavior of the protein-surfactant mixtures is Newtonian to shear rates as high as  $\dot{\gamma} = 10^4 \text{ s}^{-1}$ . Further, for the dilute concentrations of the non-ionic surfactant used in this study, the measured shear viscosity of the mixtures is nearly indistinguishable from surfactant-free BSA. We have described earlier (see Figure 1, and Sharma et al.<sup>20</sup>) how surfactant-free BSA solutions can show yield-like behavior in measurements carried out on standard torsional rheometers due to the formation of a viscoelastic film at the air-water interface. The microfluidic rheometer, on the other hand, measures the true shear viscosity of these solutions in the absence of any air-liquid interfaces. Consequently, the apparent shear thinning measured in the double gap Couette geometry (Figure 1) is not observed in the results presented in Figure 8a. The range of accessible shear rates in the microfluidic channel is dependent on the geometry of the channel as well as the dynamic range of the pressure transducers<sup>37</sup>. The black lines in Figure 8a show the operating window of the VROC device used in this study. The dependence of bulk viscosity on concentration for these dilute protein-surfactant solutions is governed by Einstein's expression for suspension viscosity<sup>50,51</sup> and for the dilute concentrations of surfactant used here, the mixed solution viscosity is only slightly higher than the surfactant-free solution. This concentration-dependent viscosity can be modeled using a charged suspension model as discussed in our previous contribution<sup>20</sup>.

On the other hand, the interfacial viscosity measured using the DWR fixture for different surfactant-protein mixtures is so low that it is indistinguishable from the instrument noise floor, as shown in Figure 8b. The black dashed line shows the minimum shear stress that can be measured by the instrument for the particular case of the DWR fixture. We find this minimum measurable stress value to be approximately a factor of ten greater than the minimum resolvable torque increment  $T_{\text{stated}}$  stated by the manufacturer ( $T_{\text{stated}} = 10^{-8} \text{ N m}$ ). It is clear from Figure 8b that for  $\dot{\gamma} \leq 3 \text{ s}^{-1}$ , the measured interfacial stress of the BSA-surfactant mixtures is in the range of the noise floor of the instrument, indicating that the addition of surfactant markedly decreases the viscosity of interfacial viscoelastic layer.

Grigoriev et al.<sup>26</sup> report that for the surfactant concentration ranges used in this study, the interfacial viscosity of Tween 80<sup>TM</sup> is  $\eta_s = 10^{-5} \text{ Pa s m}$ . Computing the stress from this value of viscosity and comparing it with the minimum stress

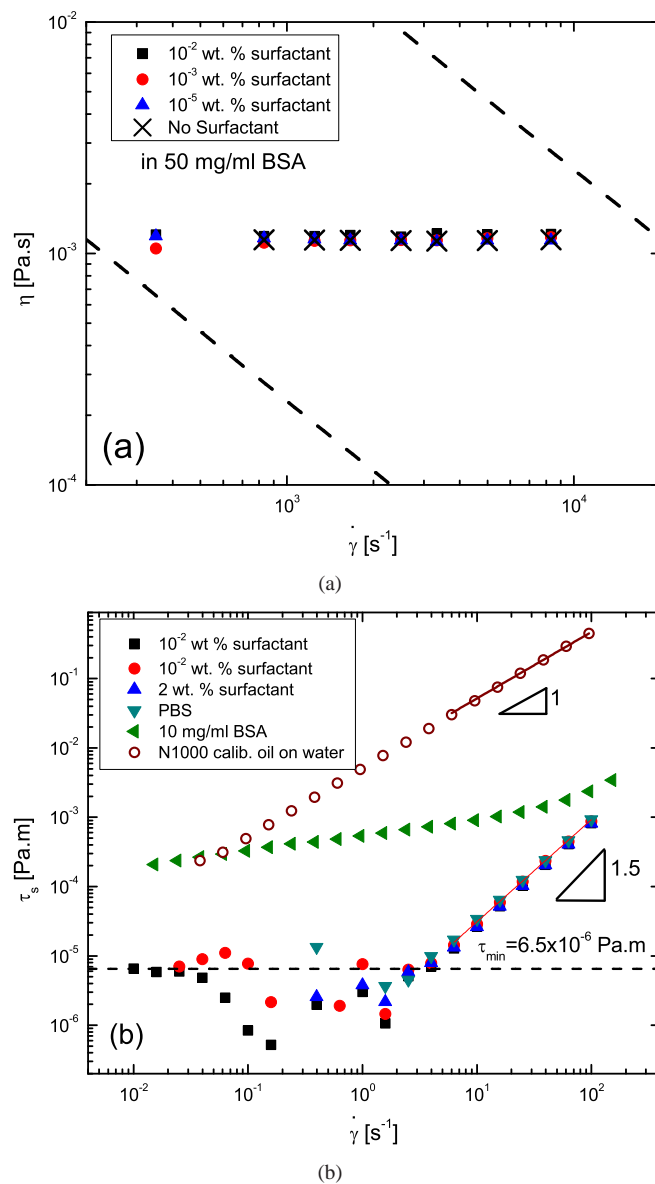


**Fig. 8** (a) Steady shear viscosity of 50 mg/ml BSA solutions with different concentrations of added surfactant measured in the interface-free microfluidic rheometer. The addition of surfactant at these concentrations makes no noticeable difference to the shear rheology of the BSA solutions in the absence of interfacial effects. (b) Interfacial steady shear viscosity measurements on 50 mg/ml BSA solutions containing different concentrations of added surfactants. The black dashed line shows the measurement limit of the instrument, and anything below this limit is indistinguishable from the noise floor. All solutions exhibit a power-law dependence of interfacial stress  $\tau_s$  on strain rate  $\dot{\gamma}$ , with  $\tau_s \sim \dot{\gamma}^{1.5}$ . This power law arises from an inertial artifact. Also shown, in hollow symbols, is the interfacial viscosity of a thin layer of Cannon N1000 Newtonian calibration oil on water. As expected for Newtonian liquids,  $\tau_s \sim \dot{\gamma}$ .

limit shown in Figure 8b, it is clear that this interfacial viscosity is too small to be measured by the DWR used in this study for  $\dot{\gamma} < 1 \text{ s}^{-1}$ . At higher shear rates, an interfacial torque contribution from the polysorbate surfactant should be measurable, but additional contributions from inertial effects in the sub-phase become increasingly dominant. It can be seen from Figure 8b that at higher shear rates the measured shear stress for all of the surfactant-BSA mixtures superpose and all follow a power law of the form  $\tau_s \sim \dot{\gamma}^{1.5}$ . The fact that the curves remain unchanged by the relatively large variation in surfactant concentration (0.01 wt.%-2 wt.%) strongly suggests that this pronounced power law response arises from an inertially-induced secondary flow of Taylor-Dean type in the sub-phase (similar power-law corrections for fluid inertia are observed in cylindrical geometries on conventional bulk rheometers<sup>52</sup>). We can define an appropriate Reynolds number for the flow induced by the DWR fixture to be  $Re_s = \rho R \dot{\gamma} a / F_\gamma \mu_{\text{sub}}$  where  $\rho$  is the density of the sub-phase,  $R$  is the radius of the ring,  $a$  is the thickness of the ring, and  $\mu_{\text{sub}}$  is the dynamic viscosity of the (Newtonian) sub-phase. Using this definition for the Reynolds number, we find that for all the protein-surfactant mixtures, as well as the pure buffer (PBS) that  $Re_s$  is greater than unity and secondary flows should be expected. A detailed computation of the resulting toroidal flow in the sub-phase is beyond the scope of this paper but the resulting inertial contribution to the interfacial stress can be extracted from the data in Figure 8b and is described by the empirical relationship  $\tau_s = 1.04 \times 10^{-6} \dot{\gamma}^{1.5}$  (with stress in Pa m and shear rate in  $\text{s}^{-1}$ ).

Also shown for comparison in this figure (hollow circles) is the interfacial shear stress as a function of shear rate for an ideal Newtonian viscous interface; which can be realized by floating a thin layer of Newtonian calibration oil (N1000, Cannon Instrument Company) carefully atop the PBS sub-phase. For this viscous interface, we achieve the desired condition of  $Bo_s \gg 1$  and the inertial contribution from the sub-phase to the torque is now negligible so that the measured stress increases linearly with imposed shear rate, as expected for a viscous Newtonian interface in the absence of inertial corrections. Baravian and Quemada have emphasized that the periodic oscillations seen at short times in creep experiments<sup>40</sup> performed on a controlled-stress rheometer necessarily imply the presence of elasticity whereas purely viscous materials do not give rise to creep ringing. We emphasize that the same holds true for interfacial creep-ringing experiments as well and oscillations are visible if, and only if, substantial interfacial elasticity is present and the system is under-damped, as described in the previous section.

This observation is underscored by the data presented in Figure 9, which shows creep experiments performed on solutions of 50 mg/ml BSA with different concentrations of added surfactant. For the two highest concentrations of sur-

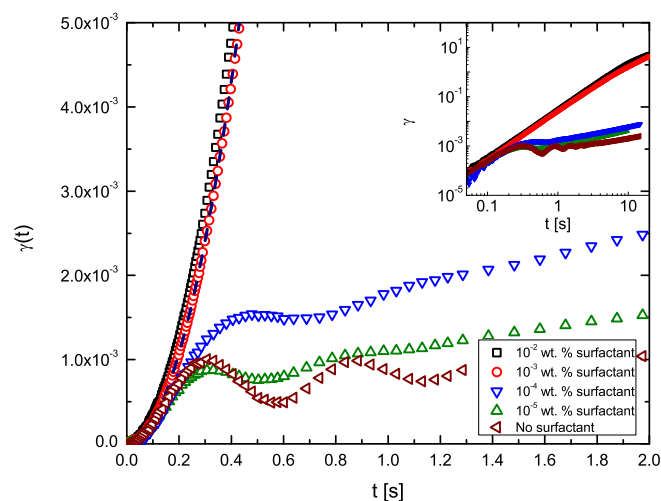


**Fig. 9** Comparison of interfacial creep ringing experiments performed on 50 mg/ml BSA solutions with different concentrations of added surfactant. Creep ringing is absent for surfactant concentrations  $c_{\text{surf}} = 10^{-2}$  wt.% and  $c_{\text{surf}} = 10^{-3}$  wt.%. The black dashed line is the expression given by the short time response equation  $\gamma(t) = (\tau_0^s b_s / 2I) t^2$  which is also the quadratic fit from the inset of Figure 3. The short time response is independent of surface elasticity and the same for all samples.

factant ( $c_{\text{surf}} = 10^{-2}$  wt.% and  $c_{\text{surf}} = 10^{-3}$  wt.%), creep ringing is completely suppressed indicating that the interface between the air and the aqueous sub-phase does not exhibit any measurable elasticity. The strain response is exactly that of a purely inertial system and is described by the expression  $\gamma(t) = (\tau_0^s b_s / 2I) t^2 + O(t^3)$ . The quadratic fit to the short time response of surfactant-free 50 mg/ml BSA shown earlier in Figure 3 is re-plotted here as a blue dashed line. Since the strain at short times is independent of the interfacial rheology, the quadratic fit from Figure 3 is unchanged, and accurately describes the data shown in Figure 9 for  $c_{\text{surf}} = 10^{-2}$  wt.% and  $c_{\text{surf}} = 10^{-3}$  wt.%.

Creep ringing is visible for the lower surfactant concentrations of  $c_{\text{surf}} = 10^{-4}$  wt.% and  $c_{\text{surf}} = 10^{-5}$  wt.%. It is evident that the change in surface viscoelastic properties happens very rapidly over a narrow surfactant concentration range ( $10^{-4} < c_{\text{surf}} < 10^{-3}$  wt.%). As before, we can estimate the values of the interfacial storage and loss moduli for the different mixtures using Equations 14 and 15. From this we determine values of  $G'_s(c_{\text{surf}} = 10^{-4} \text{ wt. \%}) = 0.015 \text{ Pa m}$  and  $G'_s(c_{\text{surf}} = 10^{-5} \text{ wt. \%}) = 0.021 \text{ Pa m}$  respectively.

To independently check these values extracted from creep ringing, small amplitude oscillatory time sweeps with the strain amplitude held fixed at  $\gamma_0 = 1\%$  for  $c_{\text{surf}} = 10^{-4}$  wt.% and surfactant-free BSA were also performed and are shown in Figure 10. Care must be taken in performing such mea-

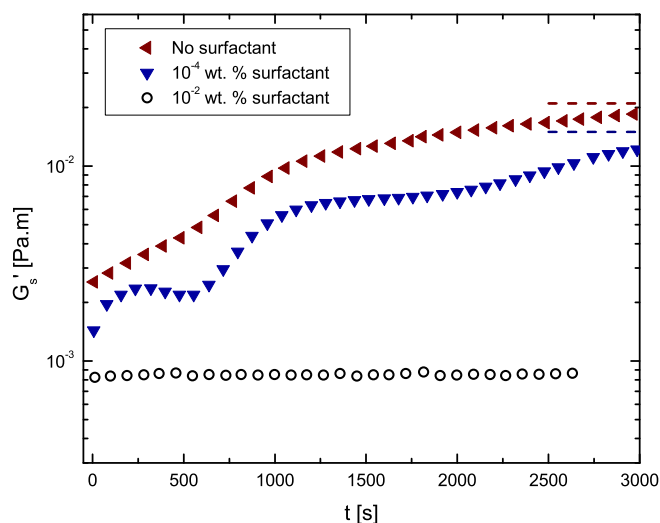


**Fig. 10** Time sweep of the interfacial storage modulus of 50 mg/ml BSA solutions with different amounts of added surfactant. The dashed lines mark the corresponding value of  $G'_s$  obtained from the creep ringing analysis. The values of  $G'_s(c_{\text{surf}} = 10^{-4} \text{ wt. \%}) = 0.015 \text{ Pa m}$  and  $G'_s(\text{no surf}) = 0.023 \text{ Pa m}$  match very well with those obtained from the creep ringing analysis. **Analysis of the raw phase angle for the mixture with  $c_{\text{surf}} = 10^{-2} \text{ wt. \%}$  shows that the surface elasticity detected by the time sweep SAOS test is an inertial artifact.**

measurements due to the temporal dynamics that arise from the competitive adsorption of the two surface-active species. The elapsed time between the loading of the sample and the initiation of the interfacial SAOS tests shown in Figure 10 is less than a minute in each case. For the protein-surfactant mixtures, similar steady state values were reached in successive measurements, but the transient approach to the steady state shows substantial variation in each test. Nonetheless, the value of the storage modulus estimated from the creep ringing in Figure 9 ( $G'_s(c_{\text{surf}} = 10^{-4} \text{ wt. \%}) = 0.015 \text{ Pa m}$ ) is in close agreement with the steady state value of the time sweep, shown in Figure 10 ( $G'_s = 0.014 \text{ Pa m}$ ).

The raw phase angle values measured during the time sweep performed on the mixture with  $c_{\text{surf}} = 10^{-2} \text{ wt. \%}$  range between  $179.3^\circ$  and  $179.7^\circ$  and the DWR response is dominated by inertia. When a time sweep SAOS test is performed on a pure DI water interface (not shown here), we again observe that the raw phase angle lies in the same range, giving an apparent reported value of  $G'_s \approx 5 \times 10^{-4} \text{ Pa m}$ . Because a pure DI water interface does not exhibit surface elasticity, the non-zero value of  $G'_s$  and the very large values of the raw phase angle indicate the dominance of inertial effects. The very small constant value of elasticity detected by time sweep on the surfactant mixture ( $c_{\text{surf}} = 10^{-2} \text{ wt. \%}$ ) is also an inertial artifact. The creep ringing experiments also demonstrate the absence

of surface elasticity through the quadratic inertially dominated response of the measured displacement at all times (see Figure 9).

The absence of creep ringing and markedly diminished interfacial viscoelasticity of the BSA/Polysorbate 80 mixtures shows that the addition of surfactant disrupts the structure formed by this globular protein at the interface. When proteins adsorb at the air/water interface, in addition to conformational intramolecular changes within the proteins<sup>11,53,54</sup> the intermolecular protein-protein interactions result in a two-dimensional network structure formation beyond a certain critical concentration<sup>6</sup>. The viscoelasticity of the interfacial layers manifested in creep ringing and SAOS experiments discussed here (Figures 3-7) is a measure of the response of the microstructure thus formed to imposed deformations. The surface topography and the location and distribution of the hydrophobic and hydrophilic moieties determine the amphiphilic character of a protein and consequently its surface activity<sup>6,11</sup>. Due to conformational constraints and improper packing, optimal orientation of these hydrophobic and hydrophilic groups at the interface is sometimes prevented and proteins do not reduce the interfacial tension as dramatically as low molecular weight surfactants which can align and organize themselves at the interface more rapidly and optimally<sup>6,10,11</sup>. However the presence of proteins imparts a substantially higher interfacial elasticity and viscosity than the corresponding low molecular weight surfactants. The higher interfacial viscoelasticity of the surfactant-free BSA solutions is seen in both interfacial measurements as well as in the apparent yielding behavior in bulk measurements.

The addition of surfactants can modify the microstructure, equilibrium and dynamic adsorption values, and the rheological characteristics of interfacial layers<sup>3,10,11,55</sup> and the interfacial properties of the mixed protein/surfactant system are also quite different from the bulk. Studies of the microstructure at the interface using Brewster Angle Microscopy or Fluorescence Microscopy<sup>56-58</sup> or by evaluating local dynamics using micro-rheology reveal the presence of considerable interfacial phase separation with localized surfactant-rich and protein-rich regions<sup>3,4,36</sup>. Several studies show that the interconnected interfacial network formed by globular proteins can be disrupted by the addition of surfactants through "orogenic displacement" as discussed in a recent review by Morris and Gunning<sup>59</sup>. The surfactant molecules that adsorb at the pre-existing protein interface begin to self-assemble into small domains, that grow in size with time and eventually disrupt the protein network. The two-dimensional microstructure created at the air-liquid interface evolves as phase separation or orogenic displacement occurs and additional conformational changes slowly take place within the protein<sup>59</sup>. Such observations can be combined with temporal measurements such as those shown in Figure 10) to understand and correlate these

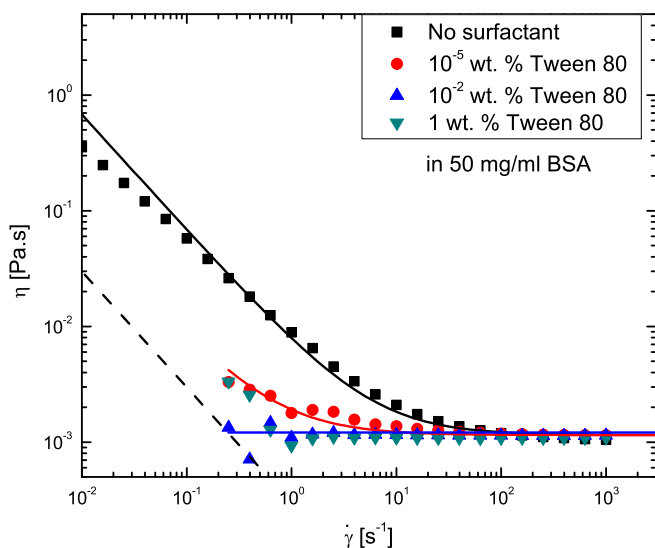


**Fig. 11** Bulk steady shear viscosity measurements performed on 50 mg/ml BSA solutions with different concentrations of added surfactants. The black line shows the minimum viscosity that is distinguishable from the noise floor for the double gap Couette geometry used in this study on the ARG2. It can be seen that the addition of surfactant dramatically reduces apparent shear thinning and yield-like behavior in the interfacial viscosity, even for relatively small quantities of surfactant ( $c_{\text{surf}} = 10^{-5}$  wt.%).

observations with the changes that occur at the scale of the individual domains in the interfacial layer. Even if the bulk concentrations of the surfactants and proteins are quite low, the species at the interface are close-packed, and independent measures of interfacial concentrations are required to correlate our reported experimental response to theoretical models, and will be necessary to understand the interfacial rheology of mixed systems.

The apparent bulk yield stress of the BSA solutions is also influenced by the addition of low molecular weight surfactants. The bulk viscosity of 50 mg/ml BSA solutions with different concentrations of added surfactant, is shown in Figure 11. The dashed line estimates the minimum measurable viscosity for the combination of the double gap Couette geometry and the controlled stress rheometer used in this study. The relationship between the minimum measurable viscosity and minimum shear rate is calculated in the same way as outlined previously, with the same value of  $T_{\text{min}} = 10^{-7}$  N m. With the addition of even a relatively small amount of polysorbate 80 ( $c_{\text{surf}} = 10^{-5}$  wt.%) to the 50 mg/ml BSA solution, the apparent bulk yield stress is lowered considerably and, for higher concentrations of surfactant, the shear thinning and the apparent yielding are nearly eliminated entirely. Again, this indicates that the mobile surfactant molecules compete with the BSA molecules for adsorption at the interface. Essentially,

the second term in Equation 1 becomes negligible in comparison with the bulk viscosity term, and therefore the reported viscosity is simply the rate-independent sub-phase viscosity  $\eta_{\infty}$ .

Grigoriev et al.<sup>26</sup> characterized the surface tension, thickness, refractive index and interfacial viscosity of mixed adsorbed layers of BSA/Tween 80<sup>TM</sup>, for  $10^{-7}$  M BSA ( $\approx 6.7 \times 10^{-3}$  mg/ml or  $\approx 0.67 \times 10^{-3}$  wt.%) and varying surfactant concentrations. They determined that above surfactant concentration of  $5 \times 10^{-6}$  M Tween 80<sup>TM</sup> ( $\approx 6.6 \times 10^{-3}$  mg/ml), the network structure formed by BSA at the interface is completely disrupted, and the resulting interfacial properties are quite similar to the properties of an interface comprising of pure Tween 80<sup>TM</sup>. It must be noted that the average value of critical micelle concentration (CMC) estimated by Grigoriev et al. (based on their measurements and literature values) is  $2 \times 10^{-5}$  M<sup>26</sup>. A wide range of surfactant properties like viscosity, conductivity, surface tension, osmotic pressure, etc. show a clear transition above the CMC, and similarly for concentrations above the CMC, the effect of added surfactant dominates the interfacial properties<sup>32</sup>. We also find that the steep drop in interfacial elasticity as a function of surfactant concentration (as documented through the creep ringing experiments pursued in the present study, cf. Figure 9) corresponds to a surfactant concentration ( $c_{\text{surf}} \approx 10^{-3}$  wt.%) that is close to the CMC values reported for Tween 80<sup>TM</sup> by Grigoriev et al. However we also note that due to the interaction with other surface-active species, both in the bulk and at the surface, the critical concentration above which surfactant properties dominate the interfacial behavior of the mixture can be above or below the CMC<sup>26,32</sup>.

The reduction in the apparent yield-like behavior on adding surfactant to the bovine serum albumin solutions indicates that the network structure formed by BSA molecules adsorbed at the liquid-air interface is progressively disrupted by the addition of the surfactant. A similar reduction in bulk viscosity has been observed by Patapoff and Esue<sup>24</sup>. Surfactants, due to their simpler structure and smaller size, are effectively more surface active than proteins, and this is revealed in the studies of adsorption isotherms as well as adsorption kinetics of surfactants in the mixed systems<sup>6,32</sup>.

## 4 Conclusions

In this paper, we have first demonstrated for the DWR fixture how the viscoelasticity of a protein interface, coupled with the finite instrument inertia of a controlled-stress instrument, can result in a damped sinusoidal strain response during interfacial creep experiments. Interfacial creep-ringing in two dimensions is shown to be analogous to its bulk counterpart, and analysis of the data presented here indicates that this free oscillatory motion can provide a quick and accurate measurement

of the interfacial viscoelastic moduli. Moreover, this technique is especially useful in extending the range of frequencies at which measurements can be performed, and measurement points where inertial effects would ordinarily overwhelm data analysis in regular frequency/strain sweeps can be accessed.

Since interfacial creep-ringing is inherently connected with the presence of an interfacial viscoelastic layer, the creep-ringing technique provides an easy way of assessing the effect of adding different concentrations of surfactants to a globular protein solution such as BSA. For concentrations of  $c_{\text{surf}} = 10^{-2}$  wt.% and  $c_{\text{surf}} = 10^{-3}$  wt.%, all visible creep ringing was found to be completely eliminated. This over-damped response indicates that the mobile surfactant molecules compete with the protein molecules for adsorption at the interface and are preferentially adsorbed. Since the low molecular weight surfactant is purely viscous and lacks measurable elasticity, no interfacial ringing is visible. We also noted from the creep-ringing experiments that the change in magnitude of viscoelastic moduli is a very sharp function of surfactant concentration over a narrow concentration range, indicating that there is not only displacement of the protein from the interface, but also disruption of the network structure formed between the protein molecules at the interface above a certain critical concentration. This is in accordance with other recent findings in literature<sup>27,60</sup> which have reported a sharp reduction of surface shear viscosity, even though a considerable amount of protein remains adsorbed at the interface. The drop in viscoelastic moduli is likely to be a combination of displacement of protein molecules at the interface, as well as the disruption of the inter-molecular network structure formed by the partially-unfolded protein molecules that form the interfacial layer<sup>5</sup>.

For lower concentrations of surfactant, interfacial creep-ringing is still observed and an estimate of the progressive reduction in the storage and loss modulus can be made using the procedures described in this paper. The complex transient response in measurements of the effective interfacial properties involving surfactant-protein mixtures reported by earlier researchers was also encountered in this study. The irreversibility of the adsorption, the presence of heterogeneous domains at the interface and the sensitivity of the structure of the interfacial layer to the adsorption history add to the complications involved in interfacial rheology measurements<sup>3,4,31</sup>. The DWR ring fixture provides a method for readily extracting an overall or effective viscoelastic property of the interface as it evolves. Microrheological techniques combined with Brewster angle microscopy will be needed to probe additional properties of these individual domains<sup>61</sup>.

We note that even a relatively small amount of the polysorbate surfactant ( $c_{\text{surf}} \geq 10^{-5}$  wt.%) suppresses the apparent bulk yield stress and shear thinning exhibited by surfactant-free BSA solutions, further emphasizing the profound influence that the interface can have on bulk rheometry. This ob-

servations provides further support for the conclusions of our previous study<sup>20</sup>, that the apparent bulk yield stress exhibited by globular protein solutions in steady shear experiments on a torsional rheometer arises due to interfacial adsorption, and not out of long-ranging weak colloidal structures as some other studies have suggested<sup>15,17,22</sup>.

The interfacial rheological properties of proteins and surfactant mixtures are often studied using different techniques to quantify the viscosity and elasticity of the interfacial layer, as these affect properties like foam and emulsion stability or mass transfer between fluids<sup>2,4,6</sup>. But the actual use and processing of food products, physiological fluids like blood<sup>62</sup>, saliva<sup>23</sup>, synovial fluid and their synthetic replacements<sup>19</sup>, cosmetics<sup>47,63</sup>, etc. requires an understanding of both their bulk and interfacial viscoelasticity. Such studies are often pursued independently of each other, but in this contribution, we show that the apparent bulk rheological response can itself change if surface-active molecules form a strong viscoelastic interfacial layer at the liquid-air interface. In this case, the extra stress contribution to the effective bulk properties originates from the stiff interfacial network formed by close-packed protein molecules. Indeed, solutions of bovine serum albumin, ovalbumins and other globular proteins<sup>15,17,18,22</sup>, acacia gum<sup>25</sup>, and monoclonal antibodies<sup>24</sup> are all examples of strong interfacial networks because their bulk rheological response measured on conventional torsional rheometers shows an apparent yield stress due to contribution of this adsorbed protein layer. While the quantitative decomposition of the interfacial and sub-phase contributions can be carried out using the additive model proposed by Sharma et al.<sup>20</sup>, in practice, the interfacial contribution can be minimized by adding low molecular weight mobile surfactants to these protein solutions. As we have shown in the present study, the concentration of non-ionic surfactant required to suppress protein adsorption and network formation at the interface is often so small that it does not affect the bulk properties of the original protein solution, at least in the present polysorbate-BSA system. Creep experiments with the interfacial DWR fixture, coupled with the creep ringing technique described above, provides a simple and rapid way of quantifying the pronounced changes in the protein/surfactant network structure formed at the liquid-air interface.

## 5 Acknowledgments

The authors would like to thank Dr. Jai Pathak of Medimmune for first making them aware of the creep ringing problem in interfacial rheometry and for valuable discussions regarding protein-surfactant interactions. We also thank Dr. Seonggi Baek at Rheosense Inc. for invaluable support with the mVROC microfluidic rheometer system.

## References

- 1 D. A. Edwards, H. Brenner and D. T. Wasan, *Interfacial Transport Processes and Rheology*, Butterworth-Heinemann, Boston, 1991.
- 2 *Interfacial Rheology*, ed. R. Miller and L. Liggieri, Koninklijke Brill NV, 2009.
- 3 B. S. Murray, *Current Opinion in Colloid & Interface Science*, 2010, **16**, 27–35.
- 4 B. S. Murray and E. Dickinson, *Food Science and Technology International*, Tokyo, 1996, **2**, 131–145.
- 5 E. Dickinson, in *Adsorbed Protein Layers in Food Emulsions*, ed. J. Sjöblom, Kluwer Academic Publishers, Dordrecht, Netherlands, 1992, p. 25.
- 6 D. Mobius and R. Miller, *Proteins at Liquid Interfaces*, Elsevier, Amsterdam, 1998.
- 7 B. Biswas and D. A. Haydon, *Proceedings of the Royal Society A: Mathematical, Physical and Engineering Sciences*, 1963, **271**, 296–316.
- 8 F. S. Ariola, A. Krishnan and E. A. Vogler, *Biomaterials*, 2006, **27**, 3404–12.
- 9 M. A. Bos and T. Van Vliet, *Advances in Colloid and Interface Science*, 2001, **91**, 437–71.
- 10 J. Krägel, R. Wüstneck, F. Husband, P. J. Wilde, A. V. Makievski, D. O. Grigoriev and J. B. Li, *Colloids and Surfaces B: Biointerfaces*, 1999, **12**, 399–407.
- 11 C. S. Kotsmar, V. Pradines, V. S. Alahverdijeva, E. V. Aksenenko, V. B. Fainerman, V. I. Kovalchuk, J. Krägel, M. E. Leser, B. A. Noskov and R. Miller, *Advances in Colloid and Interface Science*, 2009, **150**, 41–54.
- 12 J. Maldonado-Valderrama, A. Martin-Molina, A. Martin-Rodriguez, M. Cabrerizo-Vilchez, M. Galvez-Ruiz and D. Langevin, *Journal of Physical Chemistry C*, 2007, **111**, 2715–2723.
- 13 T. Peters, *All About Albumin: Biochemistry, Genetics, and Medical Applications*, Academic Press, New York, 1996.
- 14 D. C. Carter and J. X. Ho, in *Structure of Serum Albumin*, Academic Press, San-Diego, 1994, pp. 153–203.
- 15 T. Matsumoto and J. Chiba, *Journal of the Chemical Society, Faraday Transactions*, 1990, **86**, 2877.
- 16 T. Matsumoto and H. Inoue, *Chemical Physics*, 1993, **178**, 591–598.
- 17 S. Ikeda and K. Nishinari, *Biomacromolecules*, 2000, **1**, 757–63.
- 18 O. Regev, S. Vandebriel, E. Zussman and C. Clasen, *Polymer*, 2010, **51**, 2611–2620.
- 19 K. M. N. Oates, W. E. Krause, R. L. Jones and R. H. Colby, *Journal of the Royal Society, Interface*, 2006, **3**, 167–74.
- 20 V. Sharma, A. Jaishankar, Y. C. Wang and G. H. McKinley, *Soft Matter*, 2011, **7**, 5150–5160.
- 21 S. Vandebriel, A. Franck, G. G. Fuller, P. Moldenaers and J. Vermant, *Rheologica Acta*, 2010, **49**, 131–144.
- 22 S. Ikeda and K. Nishinari, *International Journal of Biological Macromolecules*, 2001, **28**, 315–20.
- 23 H. A. Waterman, C. Blom, H. J. Holterman, E. J. 's Gravenmade and J. Mellema, *Archives of Oral Biology*, 1988, **33**, 589–596.
- 24 T. Patapoff and O. Esue, *Pharmaceutical Development and Technology*, 2009, **14**, 659–664.
- 25 C. Sanchez, D. Renard, P. Robert, C. Schmitt and J. Lefebvre, *Food Hydrocolloids*, 2002, **16**, 257–267.
- 26 D. O. Grigoriev, S. Derkatch, J. Krägel and R. Miller, *Food Hydrocolloids*, 2006, **21**, 823–830.
- 27 E. Dickinson and S.-T. Hong, *Journal of Agricultural and Food Chemistry*, 1994, **42**, 1602–1606.
- 28 J.-L. Courthaudon, E. Dickinson and D. Dalgleish, *Journal of Colloid and Interface Science*, 1991, **145**, 390–395.
- 29 J.-L. Courthaudon, E. Dickinson, Y. Matsumura and D. C. Clark, *Colloids and Surfaces*, 1991, **56**, 293–300.
- 30 J. Chen and E. Dickinson, *Colloids and Surfaces A: Physicochemical and Engineering Aspects*, 1995, **101**, 77–85.
- 31 Dominique Langevin, *Mixed surfactant - polyelectrolyte layers*, Koninklijke Brill NV, 2009, pp. 303–329.
- 32 *Interactions of Surfactants with Polymers and Proteins*, ed. E. D. Goddard and K. P. Ananthapadmanabhan, CRC Press, 1993.
- 33 R. J. Mannheimer and R. S. Schechter, *Journal of Colloid and Interface Science*, 1970, **32**, 195–211.
- 34 S.-G. Oh and J. C. Slattery, *Journal of Colloid and Interface Science*, 1978, **67**, 516–525.
- 35 P. A. Wierenga, H. Kusters, M. R. Egmond, A. G. J. Voragen and H. H. J. de Jongh, *Advances in Colloid and Interface Science*, 2006, **119**, 131–9.
- 36 L. A. Pugnaloni, E. Dickinson, R. Ettelaie, A. R. Mackie and P. J. Wilde, *Advances in Colloid and Interface Science*, 2004, **107**, 27–49.
- 37 C. J. Pipe, T. S. Majmudar and G. H. McKinley, *Rheologica Acta*, 2008, **47**, 621–642.
- 38 K. Walters, *Rheometry*, Chapman and Hall, London, 1975.
- 39 R. H. Ewoldt and G. H. McKinley, *Rheology Bulletin*, 2007, **76**, 4–6.
- 40 C. Baravian and D. Quemada, *Rheologica Acta*, 1998, **37**, 223–233.
- 41 L. C. E. Struik, *Rheologica Acta*, 1967, **6**, 119–129.
- 42 R. J. Larsen, M. D. Dickey, G. M. Whitesides and D. A. Weitz, *Journal of Rheology*, 2009, **53**, 1305.
- 43 A. Jaishankar, *MSc thesis*, Massachusetts Institute of Technology, 2011.
- 44 N. W. Tschoegl, *The Phenomenological Theory of Linear Viscoelastic Behavior*, Springer-Verlag, New York, 1989.
- 45 D. Craiem and R. L. Magin, *Physical Biology*, 2010, **7**, 13001.
- 46 E. M. Freer, K. S. Yim, G. G. Fuller and C. J. Radke, *Langmuir: The ACS Journal of Surfaces and Colloids*, 2004, **20**, 10159–67.
- 47 B. Barry and B. Warburton, *Journal of the Society of Cosmetic Chemists*, 1968, **19**, 725–744.
- 48 P. Erni, E. J. Windhab, R. Gunde, M. Graber, B. Pfister, A. Parker and P. Fischer, *Biomacromolecules*, 2007, **8**, 3458–66.
- 49 D. E. Graham and M. C. Phillips, *Journal of Colloid and Interface Science*, 1980, **76**, 240–250.
- 50 S. E. Harding, *Progress in Biophysics and Molecular Biology*, 1997, **68**, 207–262.
- 51 R. G. Larson, *The Structure and Rheology of Complex Fluids*, Oxford University Press, 1999.
- 52 C. W. Macosko, *Rheology: Principles, Measurements and Applications*, Wiley-VCH, 1994.
- 53 L. G. Cascão Pereira, O. Théodoly, H. W. Blanch and C. J. Radke, *Langmuir*, 2003, **19**, 2349–2356.
- 54 K. B. Song and S. Damodaran, *Journal of Agricultural and Food Chemistry*, 1987, **35**, 236–241.
- 55 J. Maldonado-Valderrama and J. M. R. Patino, *Current Opinion in Colloid & Interface Science*, 2010, **15**, 271–282.
- 56 J. M. Rodríguez Patino, C. Carrera Sánchez and M. R. Rodríguez Niño, *Advances in Colloid and Interface Science*, 2008, **140**, 95–113.
- 57 M. M. Lipp, K. Y. Lee, A. Waring and J. A. Zasadzinski, *Biophysical Journal*, 1997, **72**, 2783–2804.
- 58 V. Rampon, C. Genot, A. Riaublanc, M. Anton, M. A. V. Axelos and D. J. McClements, *Journal of Agricultural and Food Chemistry*, 2003, **51**, 2482–2489.
- 59 V. J. Morris and A. P. Gunning, *Soft Matter*, 2008, **4**, 943–953.
- 60 R. Miller, V. B. Fainerman, A. V. Makievski, J. Krägel, D. O. Grigoriev, V. N. Kazakov and O. V. Sinyachenko, *Advances in Colloid and Interface Science*, 2000, **86**, 39–82.
- 61 J. M. R. Patino, C. C. Sánchez, M. C. Fernández and M. R. R. Niño, *The Journal of Physical Chemistry B*, 2007, **111**, 8305–13.
- 62 E. Merrill, *Physiological Reviews*, 1969, **49**, 863–888.
- 63 *Rheological Properties of Cosmetics and Toiletries*, ed. D. Laba, CRC Press, 1993.